Electronic Supplementary Information

Voltage-tunable portable power supplies based on tailored integration of modularized silicon photovoltaics and printed bipolar lithium-ion batteries

Jung-Hui Kim[a,†], Inchan Hwang[a,†], Se-Hee Kim[a], Jeonghwan Park[a], Wonjoo Jin[a],

Kwanyong Seo[a,*], Sang-Young Lee[a,b,*]

[a] *Department of Energy Engineering, School of Energy and Chemical Engineering, Ulsan National Institute of Science and Technology (UNIST), Ulsan, 689-798, South Korea.*

E-mail: syleek@unist.ac.kr; Tel: +82-52-217-2948

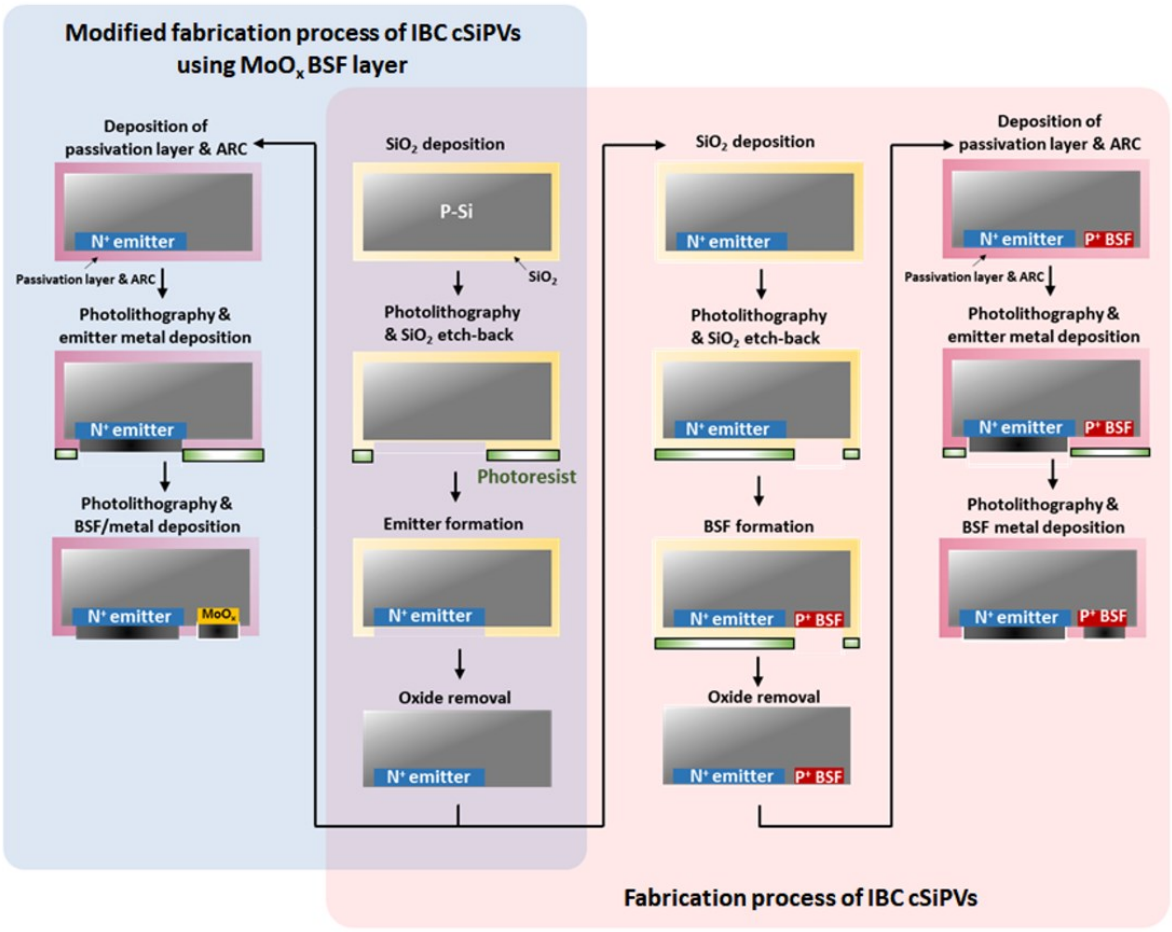

Fig. S1. Fabrication process charts of the conventional (red area) and dopant-free back-surface-field based IBC cSiPVs (blue area).

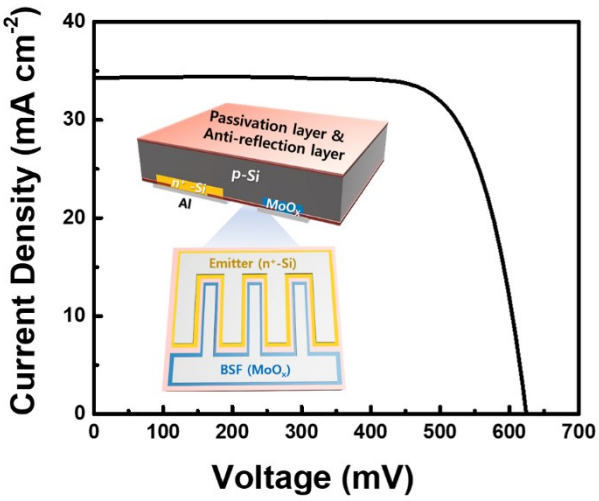

Fig. S2. Current density-voltage curve of the IBC cSiPV (inset shows the schematic image of the IBC cSiPV.

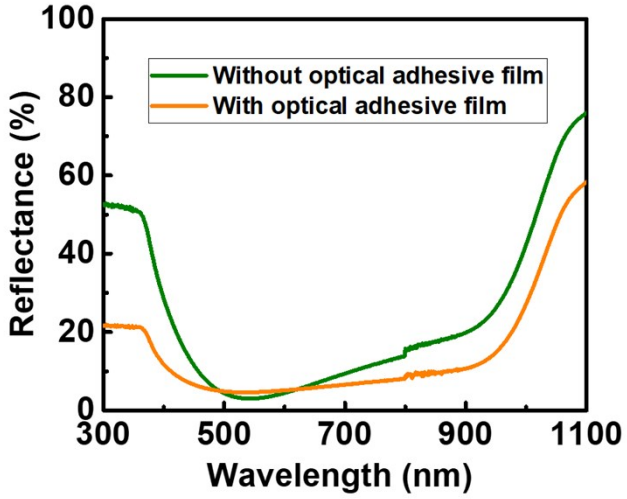

Fig. S3. Reflectance curves of the IBC cSiPV module with (red line) and without (black line) optical film.

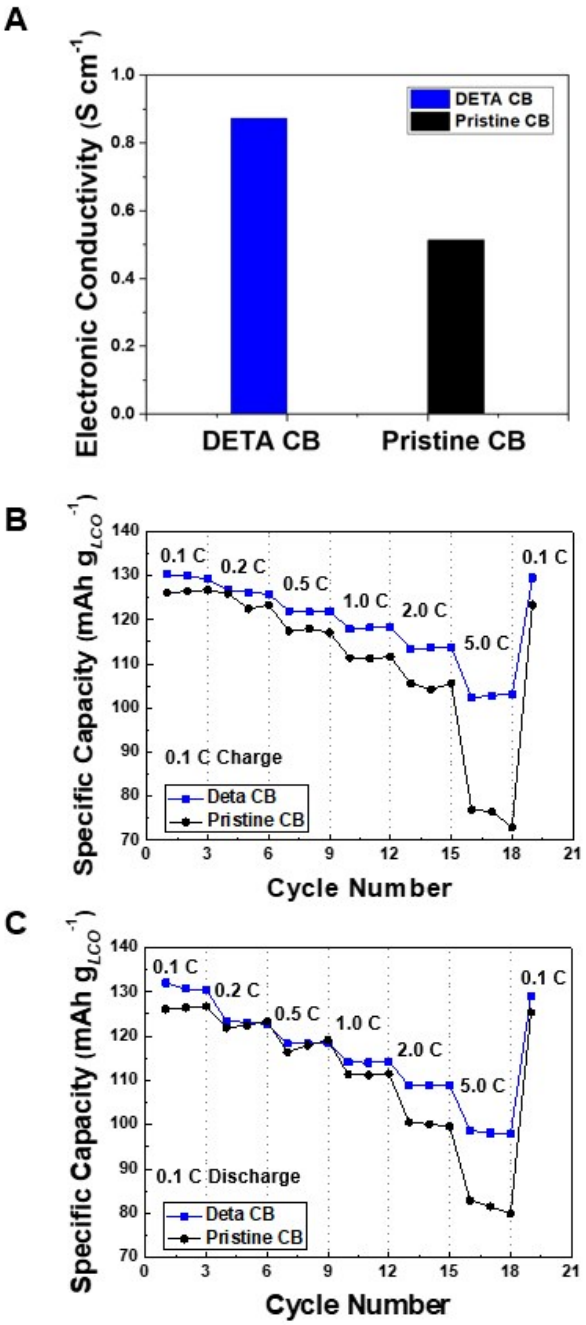

Fig. S4. Characterization of electrode using surface treated CB. (A) Electronic conductivities of the model LCO cathodes fabricated by conventional slurry casting method: pristine CB vs. DETA CB. (B) Discharge rate capability of the printed LCO half cells (Pristine CB vs. with DETA CB) over a wide range of discharge current densities from 0.1 C (= 0.08mA cm^{-2}) to 5.0 C. (C) Charge rate capability over a wide range of charge current densities (varying from 0.1C (= 0.08 mA cm^{-2}) to 5.0 C) at a fixed discharge current density of 0.1 C.

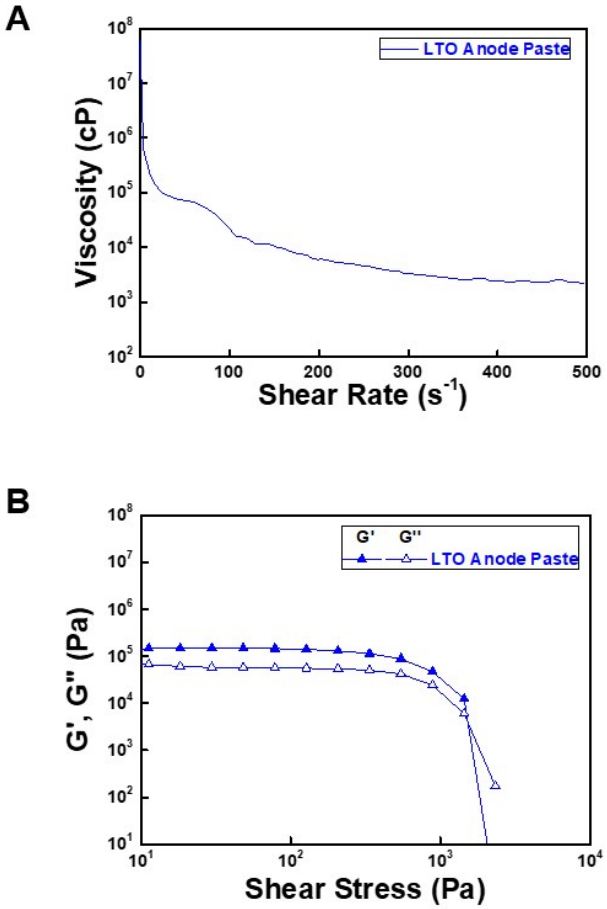

Fig. S5. Rheological properties of the LTO anode paste. (A) Viscosity as a function of shear rate. (B) Viscoelastic properties (G’ and G’’) as a function of shear stress.

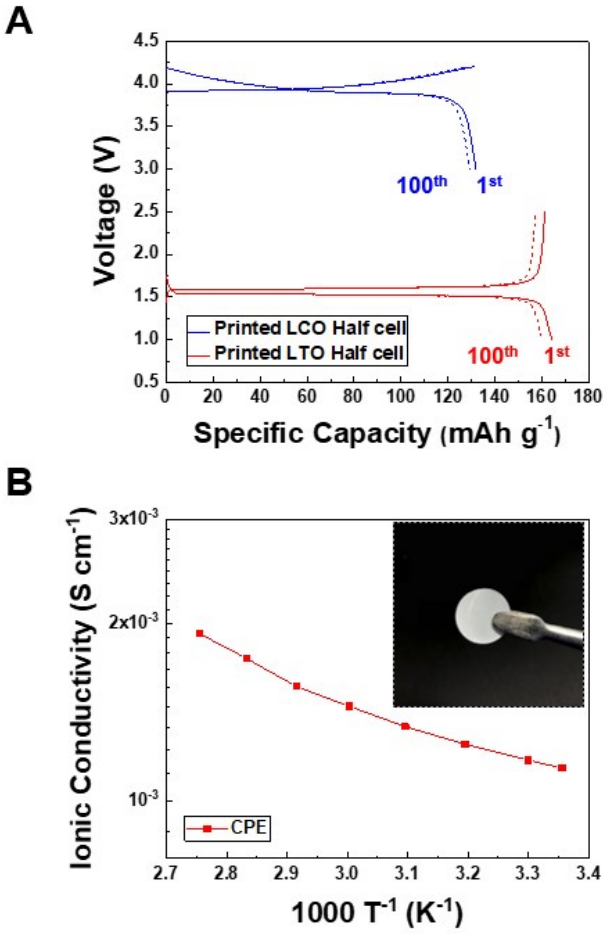

Fig. S6. Electrochemical characterization of components of bQSSB. (A) Charge-discharge profiles of the half cells containing the printed LCO cathode (or LTO anode), in which the cells were cycled at a fixed charge/discharge current density of 0.1 C/ 0.1 C at 25 ^{o}C. (B) Ionic conductivity of the CPE as a function of temperature. Inset shows a photograph of the CPE.

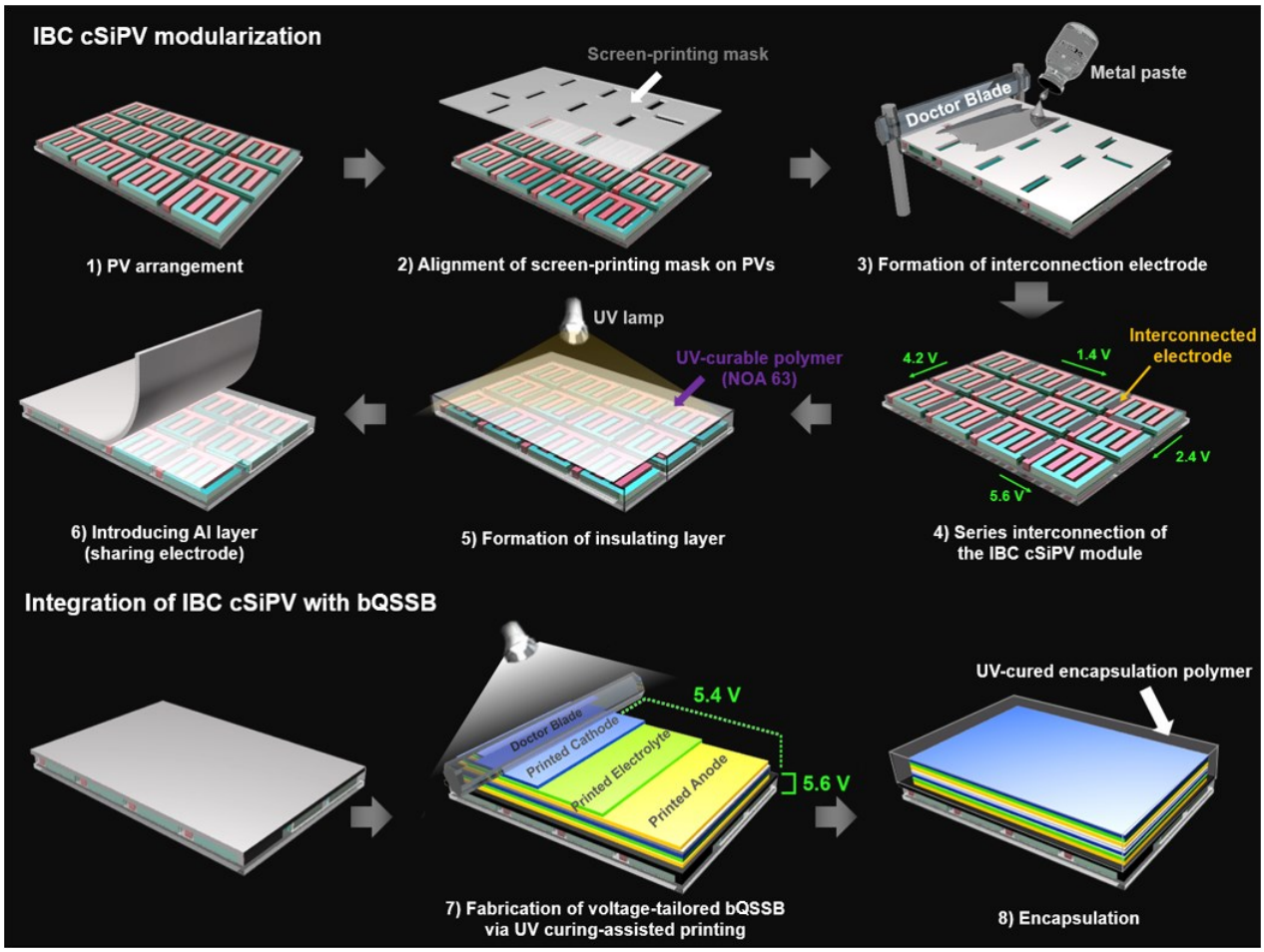

Fig. S7. Schematic illustration showing the stepwise manufacturing steps of cSiPV–bQSSB.

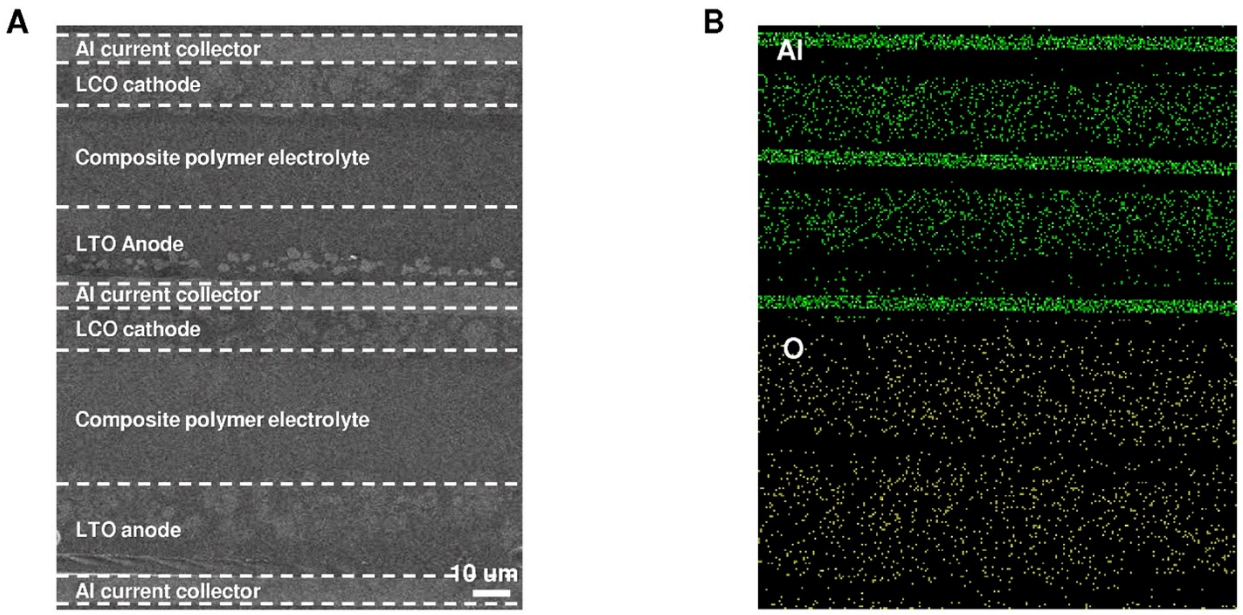

Fig. S8. Cross-sectional SEM and corresponding EDS images of the bQSSB showing the multi-layered structure.

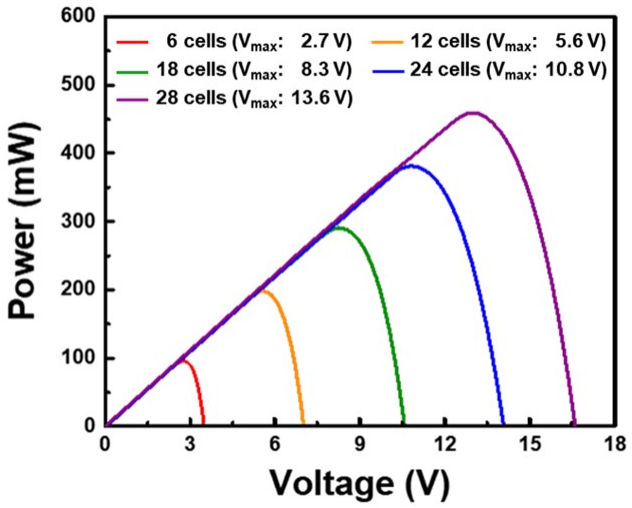

Fig. S9. Power-voltage curves of the IBC cSiPV modules as a function of the number of the series-connected PV unit cells.

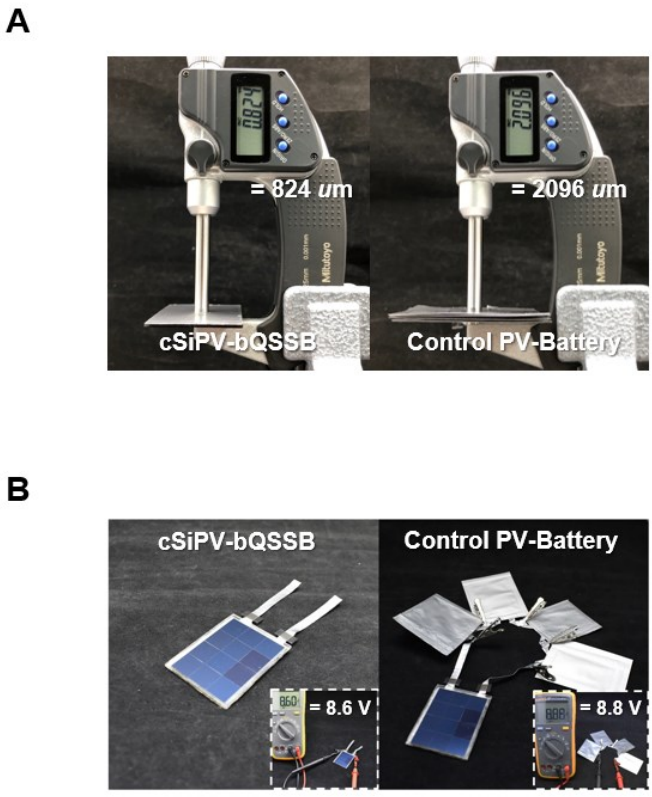

Fig. S10. Comparison of cSiPV–bQSSB and a control PV–battery (one cSiPV module with four conventional lithium-ion batteries connected in-series). (A) Thickness. (B) Photographs. Inset shows open circuit voltages of the two power systems.

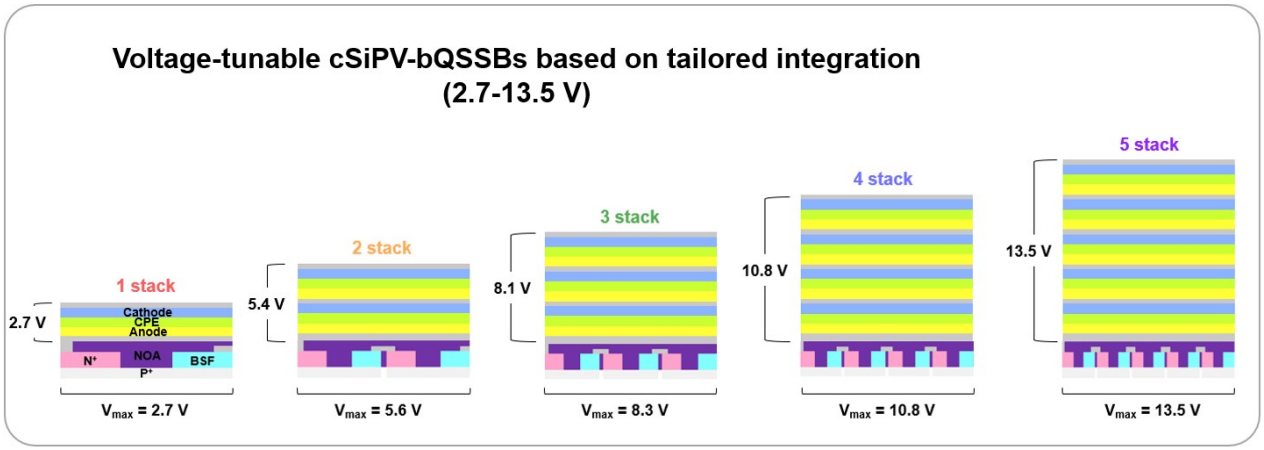

Fig. S11. Schematic illustration showing the structure of portable power supplies based on tailored integration of cSiPV-QSSBs with a wide range of operating voltage (2.7 – 13.5 V).

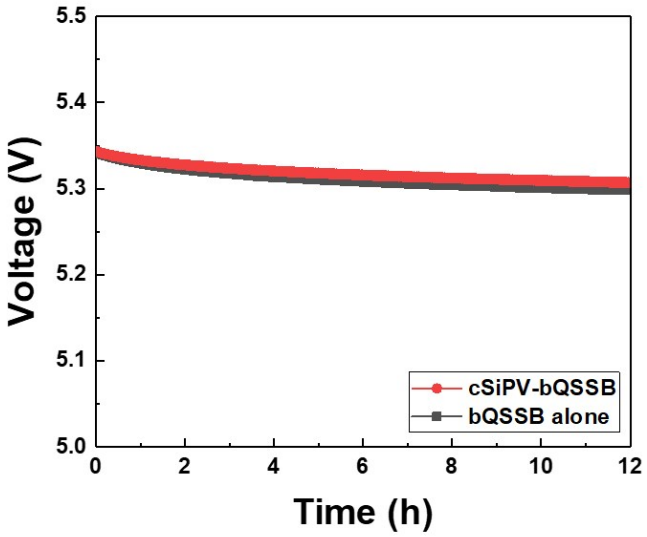

Fig. S12. OCV profiles of the cSiPV–bQSSB and bQSSB alone as a function of elapsed time.

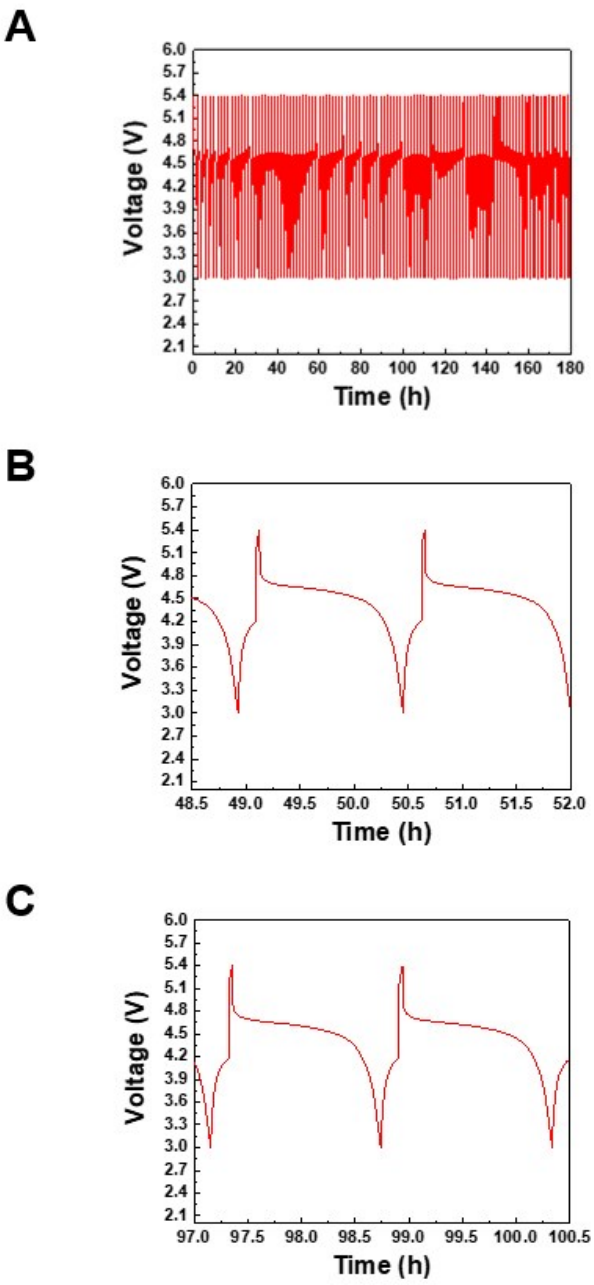

Fig. S13. (A) Photo-charge/galvanostatic discharge cycling behavior of the cSiPV–bQSSB as a function of time, in which the integrated power system was photo-charged just for 1 min under 1 Sun and galvanostatically discharged at a discharge current density of 0.1 C. Photo-charge/galvanostatic discharge profiles of the integrated power system: (B) at 50 h and (C) at 100 h.

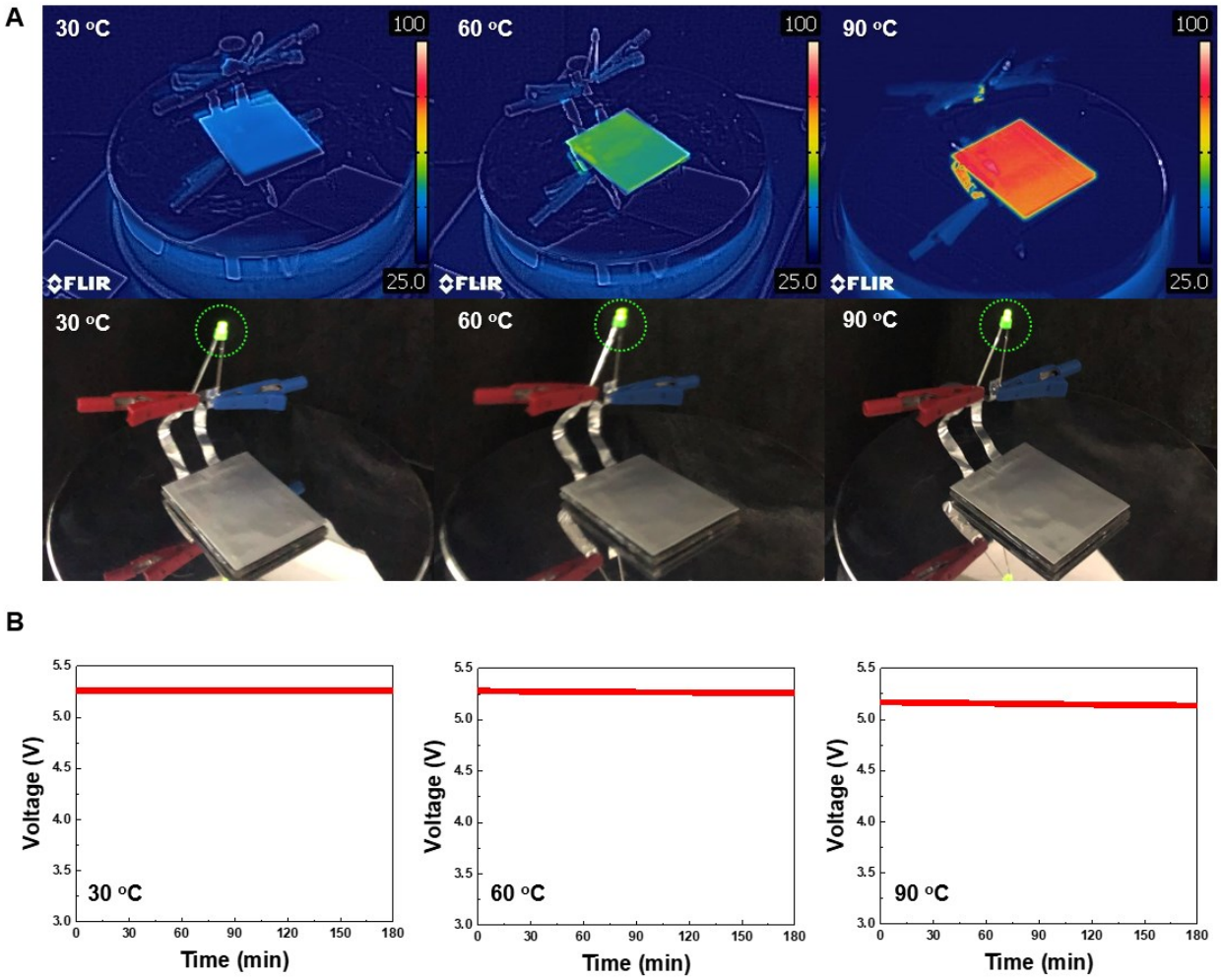

Fig. S14. Thermal tolerance of the cSiPV–bQSSB. (A) Photographs showing the dimensional stability and the normal operation of a LED after being placed on a hot plate for 3 h. (B) OCV profiles at different temperatures as a function of elapsed time.

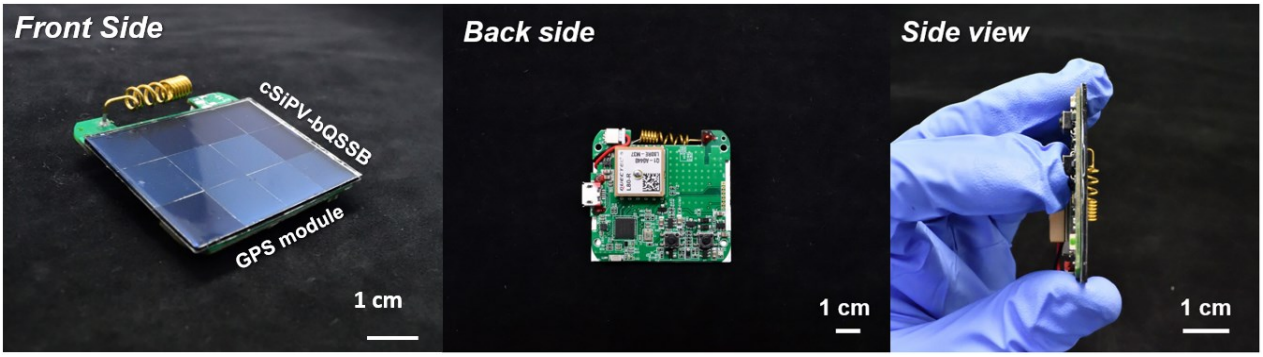

Fig. S15. Photographs of the portable GPS combined with the cSiPV–bQSSB.

Table S1. Photovoltaic parameters of the IBC cSiPV modules as a function of the number of the series-connected PV unit cells.

	6 cells	12 cells	18 cells	24 cells	28 cells
I_{sc} (mA)	36.7	37.1	37.0	37.2	37.3
V_{oc} (V)	3.5	7.1	10.6	14.0	16.6
I_{max} (mA)	34.9	35.3	35.2	35.4	33.5
V_{max} (V)	2.7	5.6	8.3	10.8	13.6
FF (%)	74.5	75.7	74.5	73.1	73.1
Efficiency (%)	15.9	16.5	16.1	15.9	16.2
Power (mW)	94.2	197.7	292.2	382.3	452.2

Table S2. Electrochemical performances of the previously reported photo-rechargeable power sources (vs. this study).

Overall Configuration	Power sources	$V_{operating}$ (V)	PCE/PSE (%)	Overall Eff (%)	Cycle (h)	Ref.
Discrete connection (via electrical wires)	PSC – LIB	2.5	12.3 / 60.0	7.36	45	(9)
	QSC – LIB	4.3	10.0 / 91.6	9.16	-	(10)
	Si-PV - LIB	7.4	3.8 / -	-	-	(11)
	Si-PV – LIB	4.2	-	-	-	(12)
	PSC – MPPT – LIB	3.0	14.2 / 77.2	9.36	20	(13)
Direct integration & Photo-assisted integration (electrochemical hybrids)	DSSC – LIB	3.3	2.0 / 41.0	0.82	1.4	(14)
	Si-PV – LIB	5.4	15.8 / 48.0	7.61	30	(15)
	DSSC – LIB	3.5	-	0.06	-	(16)
	PSC – LIB	3.0	0.03 / -	-	25	(17)
	DSSC – Li-O2	3.0	-	-	8	(18)
	DSSC – RFB	3.6	-	-	-	(19)
	DSSC – RFB	0.6	- / 62.5	-	17	(20)
	DSSC – RFB	0.8	-	-	-	(21)
	DSSC – RFB	0.8	1.7 / 78.0	1.33	-	(22)
	Si-PV – LIB	Adjustable (2.7 ~ 13.5)	16.4 / 62.0	10.20	180	This study